An Adaptive Duty-Cycle Methodology for PV Power Maximization Using a Single Variable

André A. Vidal [#1], Vítor Grade Tavares [#2], José C. Príncipe [*3]

[#] *INESC TEC – INESC Technology and Science and FEUP – Faculty of Engineering, University of Porto*
Campus FEUP, Rua Dr. Roberto Frias, 378, 4200-465 Porto, Portugal
[1] andre.vidal@fe.up.pt
[2] vgt@fe.up.pt

[*] *CNEL – Computational NeuroEngineering Laboratory*
Bldg #33, University of Florida, Gainesville, FL 32611, United States of America
[3] principe@cnel.ufl.edu

***Abstract*—This paper presents a new methodology to maximize the power output of Photovoltaic panels (PV), based on an adaptive duty-cycle methodology. The approach embeds the DC/DC converter characteristic in the cost function, allowing an optimization based on a single measured variable. Two cost functions, and respective learning rules, are derived. The first, more complex and comprehensive, traces the ground for the second which is less computational intensive and solves stability issues and implementation difficulties. It is also demonstrated that the system is asymptotically stable around the optimum duty-cycle, in the Lyapunov sense. Both methods are compared through simulations and deviations from the optimal solution are assessed.**

***Index Terms*—Adaptive Maximum Power Point Tracking, MPPT, Hebbian Learning, PV optimization**

I. Introduction

The problem of maximum power transfer in PV panels has been extensively addressed in the literature. In order to solve it, Maximum Power Point Tracking (MPPT) controllers are employed at the PV panel terminals, to drive the electrical variables to the MPP – the Maximum Power Point. Several MPPT methods have been proposed, being the most popular ones Perturb and Observe (P&O) [1], Incremental Conductance (IncCond) [2] and fractional open-circuit (or short-circuit) [3]. Their popularity arises from the implementation simplicity and good performance trade-offs. Several other methods exist, namely fuzzy control [4], neural network [5], DC link capacitor droop control [6], current sweep [7], Ripple Correlation Control (RCC) [8], among others [9]. Essentially, the MPPT algorithms vary in speed of convergence, implementation complexity, number of sensed variables, steady-state misalignment, need for parametrization (*prior* plant knowledge) and the type of digital or analog blocks [10].

In order to control PV panels such that they operate at their MPP, DC/DC (or DC/AC) converters are connected at the panel terminals, which in turn are connected to a load. The converter sources a DC output voltage and current whose magnitudes are controllable via the duty-cycle parameter D, using circuit elements that, ideally, do not dissipate power. A conceptual view of this configuration is shown in Figure 1. The output/input voltage gain depends on the topology of the converter, whose ideal expressions are shown in Table I for three types of converters. The conversion ratio, hereafter denoted as $M(D)$, is defined as the ratio of the DC output voltage (V_{out}) to the DC input (V_{in}) voltage, under steady-state conditions (assuming continuous conduction mode of the converter). Therefore, it follows that:

Table I: Different converter topologies and their respective conversion ratios

Converter	$M(D)$
Buck	D
Boost	$\frac{1}{1-D}$
Buck-boost	$-\frac{1}{1-D}$

$$M\left(D\right) = \frac{V_{out}}{V_{in}} \tag{1}$$

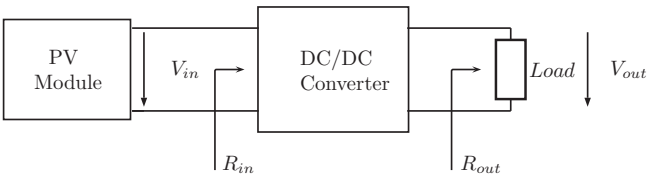

Figure 1: A conceptual view of the system setup approached in this paper.

Except for losses in the converter (modelled through the efficiency factor η), the delivered power P_{in} is the same as the output power P_{out}. Therefore one can obtain a relationship between input and output impedances, as follows:

$$\begin{aligned} P_{in} &= \eta P_{out} \\ \frac{{V_{in}}^2}{R_{in}} &= \eta \frac{\left(M\left(D\right).V_{in}\right)^2}{R_{out}} \\ \frac{1}{R_{in}} &= \left[\frac{\eta}{R_{out}}\right] M(D)^2. \end{aligned} \tag{2}$$

This last expression provides a fundamental relationship between impedances, which forms the basis of this paper.

II. Cost Functions and derivations of the learning rules

A. First Rule

In order to mathematically formulate the power maximization problem for the PV modules, a proper *cost function*, here denoted as J, must be defined. Once defined, a proper methodology for adapting the free parameters has to be developed to achieve the goal of that cost function. It is clear that such free parameters, here refer desirably to a single parameter – the duty-cycle of the DC/DC converter. This way, no other control loops are necessary, such as the normally used PI controller when voltage or current is chosen as the control variable. Moreover, such cost function must, in the control variable domain, match the PV power maxima. Given a resistive load, the power delivered to it is given by V_{in}^2/R_{in}, which using (2) can be modelled in the cost function as follows:

$$\begin{aligned} J(D) &= \underbrace{{V_{in}}^2}_{\mathbf{x}} \underbrace{\left[\frac{\eta}{R_{out}}\right]}_{\text{Scaling factor}} M(\underbrace{D}_{\mathbf{w}})^2 \\ &\propto {V_{in}}^2 M(D)^2 \end{aligned} \tag{3}$$

Note that we have assumed for now that η is a constant term that does not depend on D, so it is solely a scaling factor not affecting the $J(D)$ maxima in its input domain. The R_{out} term also does not depend on D, therefore one can say that the $\left[\frac{\eta}{R_{out}}\right]$ term is solely a scaling factor, and since it is always positive, it can be removed from $J(D)$. This cost function can be interpreted as a combination of the input – x, assigned to the voltage squared, and a weight – w, which is to be adapted through the $M(.)^2$ non-linearity. Note that despite $J(D)$ does not estimate the power curve directly, it "travels" along a scaled version of it (scaled by $\frac{\eta}{R_{out}}$), however both curves share the same optimum D^* (assuming that η does not depend on D). This method offers great advantages, since it is employing the duty cycle directly in the DC/DC converter and requires the measurement of only voltage. Therefore any external controller and/or current sensors are not required, reducing the overall complexity drastically. Equation (3) is differentiated with respect to D and used to update the duty cycle directly using the traditional stochastic gradient approach [11], yielding:

$$\frac{\partial J(D)}{\partial D} = \frac{\partial x}{\partial D} M(D)^2 + 2x.M(D)\frac{dM(D)}{dD} \tag{4}$$

A general (in the DC/DC converter sense) update rule can now be easily obtained, where n is the iteration index, and ε is the step-size:

$$D[n+1] = D[n] + \varepsilon \frac{\partial J(D)}{\partial D}[n] \tag{5}$$

Since $\frac{\partial x}{\partial D}$ is not known a-priori, as it depends on the PV characteristic, it can be approximated by the temporal differences of x and D, $\frac{\partial x}{\partial D}[n] = \frac{\partial x}{\partial t}/\frac{\partial D}{\partial t}[n] \approx \Delta x/\Delta D$. Table II shows how this rule can be applied to the different type of converters referred earlier.

Table II: Learning Rules I for three different converter typologies

Converter	$\frac{\partial J(D)}{\partial D}[n]$
Buck	$\left(\frac{\Delta x}{\Delta D} D[n]^2 + 2x[n].D[n]\right)$
Boost	$\left(\frac{\Delta x}{\Delta D}\frac{1}{(1-D[n])^2} + 2x[n].\frac{1}{(1-D[n])^3}\right)$
Buck-boost	$\left(\frac{\Delta x}{\Delta D}\frac{1}{(1-D[n])^2} + 2x[n].\frac{1}{(1-D[n])^3}\right)$

Figure 2a shows the behaviour of the controller, when the controller is employing the developed learning rule, for different ε values, namely: $\varepsilon_1 = 1\cdot10^{-7}$, $\varepsilon_2 = 2\cdot10^{-7}$, $\varepsilon_3 = 3\cdot10^{-7}$, $\varepsilon_4 = 4\cdot10^{-7}$, $\varepsilon_5 = 5\cdot10^{-7}$. The plant comprises a PV panel capable of delivering nearly 8W of power, coupled with a *Boost* DC/DC converter with $R_{out} = 100\Omega$. When the adaptation starts (with an initial value of $D[0] = 0.5$), the gradient (green curves in the bottom-left plot of the same figure) increases exponentially as the controller approaches the optimum, reaching then its peak value. At this point, the present value of duty cycle is already very close to the optimum (approximately 80% of the optimum value). Then, the gradient abruptly reverses its trend in order to compensate this effect, "swinging" ultimately around a zero value when the system has reached the optimum. Very large discrepancies between the initial and maximum values of the gradient are noticeable, which in addition are not located in desirable locations. In fact, the cost function should ideally be a paraboloid surface where its gradient is continuously weakening as the system reaches the optimum.

B. Second Rule: Improvements in the cost function

This effect can be overcome if one uses a proper *basis function* $\phi(u)$ that is monotonically increasing and differentiable with respect to its input domain. In this case, a new criterion function $\hat{J} = \phi(J(D))$ can be defined, where the maximums of $\hat{J}$ and J are located at the same D^*. Thus, using the chain rule, a new learning rule can be obtained through:

$$\frac{\partial \hat{J}}{\partial D} = \left.\frac{\partial \hat{J}}{\partial \phi}\right|_{u=J(D)} \frac{\partial \phi}{\partial D} \tag{6}$$

The previously undesirable effects are attenuated when the employed ϕ function moves the inflection point of $\hat{J}$ (IP) away from its original position, in the D sense, i.e. away from the maximum of J, resulting in a smoother behaviour. Figure 3 shows the $\hat{J}$ function when functions of the form $\phi(u) = -e^{-\alpha.u}$ are employed. The top part shows the $\phi(u)$ curves for α values of 0.005, 0.02 and 0.1. The middle figure shows the original cost function (for the same previous scenario) and its IP in a green square labelled as "Original IP". Three others IPs are shown for the corresponding α values.

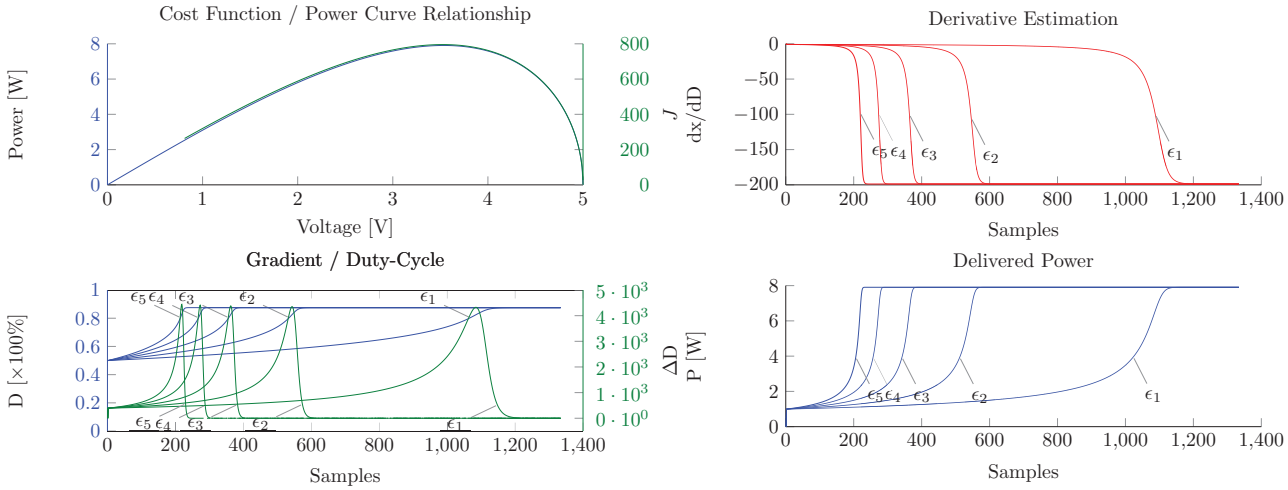

(a) Results when applying Rule I.

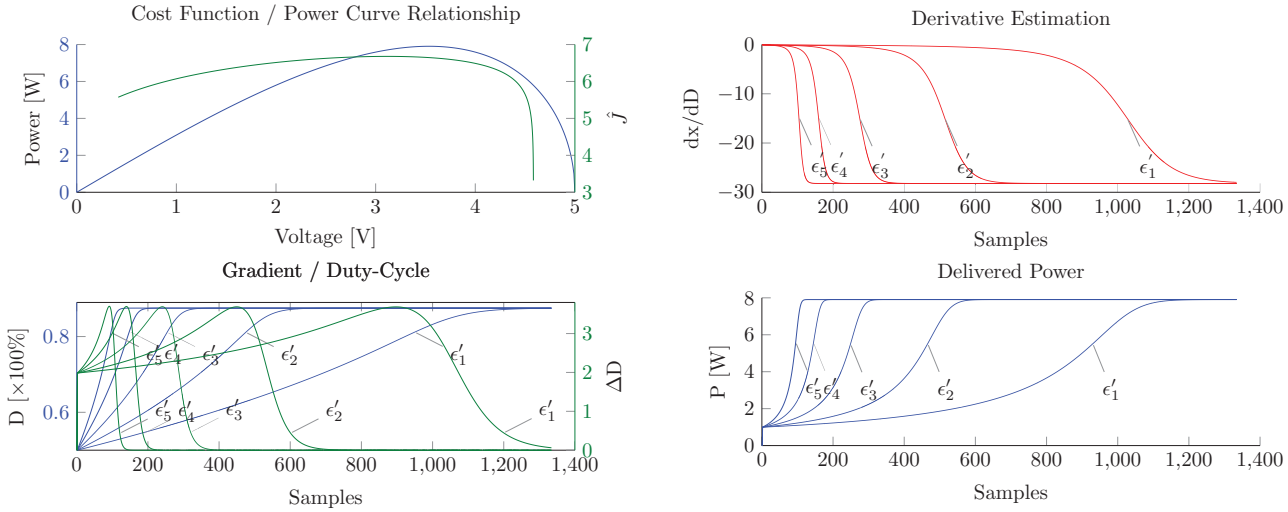

(b) Results when applying Rule II.

Figure 2: Plot of relevant variables during adaptation using rules I and II when different step-sizes are considered. On both plots, the upper left part shows the power and cost functions with respect to voltage; the right upper part shows the derivative $\frac{\partial x}{\partial D}$; the bottom-left and bottom-right parts show respectively, the gradient (along with the duty-cycle) and power curves.

They were placed on the same blue curve for visualization purposes (note that $\hat{J}$ is not of the same magnitude as J). Finally, the bottom figure shows a scaled version of the gradient of $\hat{J}$, which decreases where the IPs are located. One can easily conclude that, the "flatter" the ϕ function is in the codomain of $\hat{J}$, the more the respective IP moves away from the maximum of J.

Unfortunately, the computational complexity of the system increases significantly if ϕ functions in the previously form were to be used. However, one interesting choice for $\phi(u)$ is the $log(.)$ function, which has the double advantage of moving the IP to a more desirable position (see Fig. 4), and at the same time because of its propriety of transforming the logarithmic product into a sum. Therefore, defining $\hat{J}(D) = ln\left\{x(D)\,M(D)^2\right\}$, the gradient expression becomes:

$$\frac{\partial \hat{J}}{\partial D}(D) = \frac{\partial x(D)}{\partial \mathrm{D}}\frac{1}{x(D)} + 2\frac{dM(D)}{dD}\frac{1}{M(D)} \tag{7}$$

Since $x(D) = V_{in}(D)^2$, the gradient expression can be further simplified, eliminating the need to obtain the square of $x(D)$. Replacing $x(D) = V_{in}(D)^2$ in the gradient expression, one obtains:

$$\frac{\partial \hat{J}}{\partial D}(D) = 2\frac{\partial V_{in}(D)}{\partial \mathrm{D}}\frac{1}{V_{in}(D)} + 2\frac{dM(D)}{dD}\frac{1}{M(D)} \tag{8}$$

Table III shows this adaptation rule when applied to the very same converters (note that the 2 scalar was dropped and

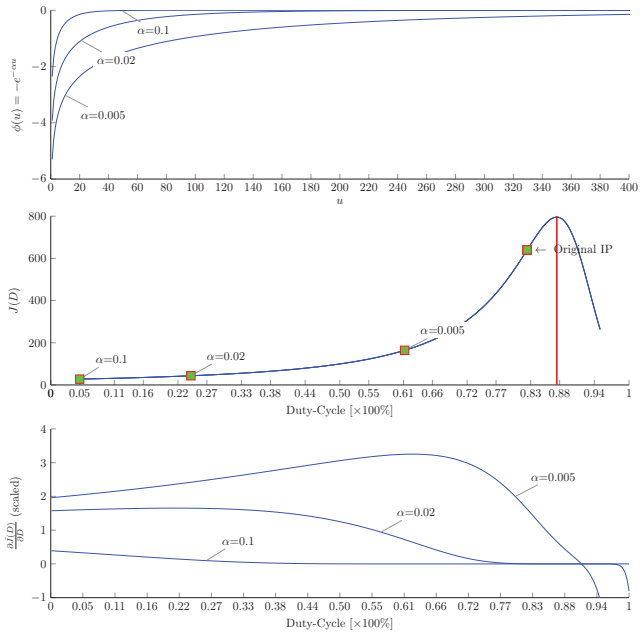

Figure 3: $\hat{J}$ features when $\phi(u) = -e^{-\alpha.u}$ for three values of α. The top part shows the $\phi(u)$ curves. The middle part shows the original IP of J, and three other IPs of $\hat{J}$ are placed on the J curve. The bottom part shows the gradient curves.

Table III: Learning Rules II for three different converters

Converter	$\frac{\partial \hat{J}(D)}{\partial D}[n]$
Buck	$\left(\frac{\Delta V}{\Delta D}\frac{1}{V[n]} + \frac{1}{D[n]}\right)$
Boost	$\left(\frac{\Delta V}{\Delta D}\frac{1}{V[n]} + \frac{1}{1-D[n]}\right)$
Buck-boost	$\left(\frac{\Delta V}{\Delta D}\frac{1}{V[n]} - \frac{1}{1-D[n]}\right)$

incorporated in the step-size). It is evident that the expressions are drastically simpler than the formers shown in Table II, especially because square and cubic terms disappear. This subsection introduced that any new rule can be obtained from equation (6), leading to a controller where J and $\hat{J}$ are computed through $\phi(u)$. However, it should be highlighted that this is not carried out explicitly when $\phi(u) = log(u)$, as this basis function leads to a special case for the learning rule.

Apart from reducing the complexity of the adaptation rule, the optimization with the $\hat{J}$ also improves the controller stability significantly. Figure 2 faces the adaptation results obtained when the first adaptation rule was used, against the results obtained for $\hat{J}$, in 2a and 2b figures respectively. Note that the plant was set exactly with the same parameters, and the learning rates were set so that the time constant of adaptation is approximately the same for both scenarios, namely: $\varepsilon'_1 = 0.4 \cdot 10^{-4}$, $\varepsilon'_2 = 0.8 \cdot 10^{-4}$, $\varepsilon'_3 = 1.5 \cdot 10^{-4}$, $\varepsilon'_4 = 2.6 \cdot 10^{-4}$ and $\varepsilon'_5 = 4.0 \cdot 10^{-4}$.

As opposed to the first scenario, the gradient is much

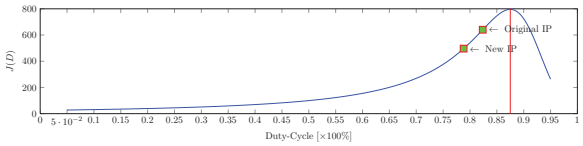

Figure 4: Displacement of the IPs when the original learning rule is used and when $\hat{J}$ is used (for $\phi(u) = ln(u)$). The green squares represent respectively, the IP of J (original IP in the figure) and the IP of $\hat{J}$ (New IP in the figure), placed on the same curve for visualization purposes.

smoother, consequently smoothing the system response significantly. Also, the discrepancies between the initial and maximum values are noticeable small when compared to the first scenario. This allows a higher speed of convergence, because in the time domain, the first rule would become unstable at some point before the second one (implying that the step-size had to be reduced, reducing consequently the adaptation speed). Moreover, using $\hat{J}$ reduces the magnitude of the gradient, so larger step-sizes must be used in order to achieve the same time-constants. This eases a practical implementation of the system, because of limited numerical resolution.

C. Stability Analysis

The derived update rule will now be proven to show global asymptotic stability around the optimum duty cycle D^*, using Lyapunov theory. It will be derived for a *boost-converter* for illustrative purposes, without loss of generality to any other type of converters.

Proof: The learning rule updates the duty-cycle values through time, as stated in (9). It can also be written as an approximation of the time-derivative of D, as (10) shows, being T the sampling step. (Note that dots on variable names refer to their derivatives with respect to time)

$$D_{i+1} = D_i + \epsilon \frac{\partial \hat{J}}{\partial D} \tag{9}$$

$$\dot{D} \approx \frac{\partial \hat{J}}{\partial D}\frac{1}{T} \tag{10}$$

Assume that T is sufficiently small so that the former inequality is assumed equal. Lyapunov conditions for stability hold at the origin of dynamic systems. Since this aims at proving that the system is globally stable around some point (the optimum D^*), a change of variables must be carried out. Let the notion of error be introduced as $e(t) = D(t) - D^*$, where $D(t)$ is the duty cycle at some time instant t, and D^* is the optimum duty-cycle for the PV system. A differential equation for this system can be obtained as follows:

$$\dot{D} = f(D,t) = \frac{\epsilon}{T}\left(\frac{dV}{dD}(D)\frac{1}{V(D)} + \frac{1}{1-D}\right) \tag{11}$$

Time-differentiating e, one obtains $\dot{e} = g(e,t) = f(D^* + e, t) - f(D^*, t)$. Since $D = D^*$ implies $\dot{D} = 0$, the second

part of this equation is $f(D^*,t)=0$. Therefore the stability on the origin of the following system is to be analysed:

$$\dot{e}=\frac{\epsilon}{T}\left(\frac{dV}{dD}(D^*+e)\frac{1}{V(D^*+e)}+\frac{1}{1-D^*-e}\right) \quad (12)$$

Let us introduce the following Lyapunov-candidate function:

$$V(e)=\frac{1}{2}e^2 \quad (13)$$

Differentiating this function with respect to time one gets:

$$\dot{V}(e)=e\dot{e}=e\frac{\epsilon}{T}\frac{dV}{dD}(D^*+e)\frac{1}{V(D^*+e)}+e\frac{\epsilon}{T}\frac{1}{1-D^*-e} \quad (14)$$

At this point, Lyapunov conditions need to be verified for these functions to check if stability holds, i.e., if $V(e)$ is positive definite and $\dot{V}(e)$ is negative definite. One immediately concludes that such propriety holds for $V(e)$, and the same can be easily done for $\dot{V}(e)$, as will now be shown. Both terms in $\dot{V}(e)$ multiply by e, thus implying $\dot{V}(0)=0$. Therefore it will be shown that the sum of these two terms is always negative.

Dealing first with the first term, $\frac{dV}{dD}$, it can be rewritten using the chain rule as follows:

$$\frac{dV}{dD}=\frac{\partial V}{\partial f}\frac{\partial f}{\partial D} \quad (15)$$

Suppose that the I-V curve of the PV module to be controlled is modelled through a monotonically decreasing function (in physical terms this means that no "shading" effects are present) and the PV is always operating as source (V is always positive). This implies that $\frac{\partial f}{\partial V}$ is always negative. Conversely the same holds for $\frac{\partial V}{\partial f}$. As for the $\frac{\partial f}{\partial D}$ quantity, note that since we are dealing with a boost converter, the input impedance is ideally given by $R_{in}=R_{out}\left(1-D\right)^2$. This implies that in extreme scenarios, the input resistance is either 0 (for $D=1$) or R_{out} (for $D=0$). Since $\left(1-D\right)^2$ is monotonic, the input resistance decreases monotonically between these two extreme points, then $\frac{\partial f}{\partial D}$ is positive. These considerations imply finally that $\frac{dV}{dD}\frac{1}{V}$ is negative $\forall D\in(0,1)$.

Regarding the second term, note that the function changes its sign on its asymptote, located at $e=1-D^*$. For smaller values of e, it is negative, and positive for bigger values of e. This observation is sufficient, since $e=1-D^*$ corresponds to $D=1$, therefore $\dot{V}(e)$ is proven to be positive definite. In fact, it is not globally positive definite, which was expected since solutions with $D>1$ are not feasible, and this Lyapunov function mimics exactly that converter constraint. However, it has been proven that within the feasible operating points of the system, global stability is ensured by this MPPT controller. ■

D. Practical Considerations

Regardless of the method to be applied, $\frac{\partial x(D)}{\partial \mathrm{D}}$ is never directly available, hence its value must be estimated and special care must be taken. As stated earlier, it can be estimated by the temporal differences, in the following way:

$$d\left[n\right]=\frac{\dot{\mathrm{V}}\left[n\right]}{\dot{\mathrm{D}}\left[n\right]} \quad (16)$$

where $\dot{\mathrm{V}}\left[n\right]$ and $\dot{\mathrm{D}}\left[n\right]$ are respectively, the time derivatives of V and D at time instant n. These derivatives can be estimated, in the simpler way, by taking the temporal differences, e.g., $\dot{\mathrm{V}}\left[n\right]=\Delta V\left[n\right]=V\left[n\right]-V\left[n-1\right]$ and $\dot{\mathrm{D}}\left[n\right]=\Delta \mathrm{D}\left[n\right]=D\left[n\right]-D\left[n-1\right]$. A more convenient (but not necessary) way to obtain a reasonable estimate for $\frac{dV}{dD}$, is to pre-filter the quantities $\dot{\mathrm{V}}\left[n\right]$ and $\dot{\mathrm{D}}\left[n\right]$ using for instance a differentiator operator of the form

$$\left(1-\frac{\alpha}{s+\alpha}\right)\overset{z}{\leftrightarrow}\alpha\left(1-\alpha\frac{z}{z-b}\right) \quad (17)$$

where s is the Laplace variable, z is the transformation variable associated with the Z-transform, $\alpha>1$ is a smoothing factor and $b=e^{-\alpha T}$, where T is the sampling period. A discrete implementation of (17), takes the following form:

$$\begin{aligned} y\left[n+1\right]&=by[n]+\left(1-b\right)x[n]\\ \dot{x}\left[n+1\right]&=\alpha(x\left[n\right]-y\left[n+1\right]) \end{aligned} \quad (18)$$

where x is the variable that is to be time-differentiated.

This derivative takes a non-zero value in steady state (equating (7) to zero gives $\left(\frac{dV}{dD}\right)^*=-V^*M(D^*)$, where $(.)^*$ refers to the optimum value of the respective variables), so its proper estimate is of major importance. Since the variations in D are very small in steady-state, this estimate becomes very unstable. A simple saturation operator is desirable, where its bounds can be set close to the theoretical $\left(\frac{dV}{dD}\right)^*$, if available.

E. Consequences of the non-constant behaviour of the DC/DC converter

During the derivation of the cost functions, the efficiency η was assumed constant. However, it is in fact a function of D - the independent variable, as well as controller parameters. The analysis and conclusions of the consequences of such assumption will be made for a DC/DC *boost* converter, but analogous results hold for other DC/DC typologies. According to [12], the efficiency of a *boost* converter is as follows:

$$\eta\left(D,r_s,r_p,R\right)=\frac{R}{R+r_p}\frac{\left((R+r_p)^2-R(R+2r_p)D\right)D'}{r_s(R+r_p)+Rr_pD'+R^2D'^2} \quad (19)$$

where R,r_s,r_p are respectively, the load resistance, the internal resistance of the input inductor and equivalent series resistance of the output filter capacitor; and $D'=(1-D)$. Note that the switches were still assumed ideal. Figure 5 shows some curves of this function for different values of the load impedance, for the same $r_s=0.10\Omega$ and $r_p=0.10\Omega$.

In fact, the learning rules derived previously could have incorporated this effect, which would have leaded to the following equations for both rules:

$$\begin{aligned} \frac{\partial J\left(D\right)}{\partial D}=x\Bigg[&\frac{\partial\eta}{\partial D}\frac{1}{\left(1-D\right)^2}\\ &+\eta\frac{2}{\left(1-D\right)^3}\Bigg]+\frac{\partial x}{\partial D}\left(\eta\frac{1}{\left(1-D\right)^2}\right) \end{aligned} \quad (20)$$

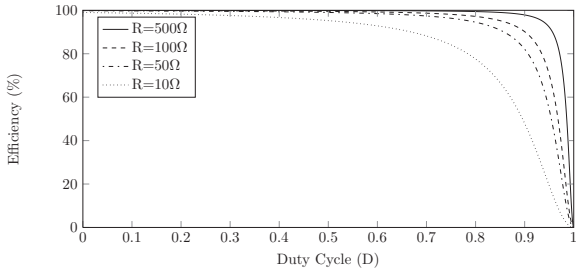

Figure 5: Different efficiency curves for the *boost* DC/DC converter when different R_{out} values are considered.

$$\frac{\partial \hat{J}(D)}{\partial D} = 2\frac{\partial V}{\partial D}\frac{1}{V} + \frac{\partial \eta}{\partial D}\frac{1}{\eta} + 2\frac{1}{1-D} \tag{21}$$

It was assumed that $\eta(D) = constant$, hence $\frac{\partial \eta}{\partial D} = 0$, which leads to the same results derived previously. The incorporation of this effect in the learning rule, would however lead to heavy computational costs, and it is of great interest to keep the computations low. Moreover, the converter parameters in (19) are not always available, and can be even time-varying (which is the case for R). This affects the magnitude of the cost function curve in a non-constant way, affecting the maxima position. However, the deviations are in general very small, lower than the ripple around D^* which naturally arises through any perturbation method.

III. Simulations

The simulated setup was performed in Matlab, comprising a static plant, in the sense that the model of the attached DC/DC converter was static, hence no transients due to the DC/DC converter are present. This approach decorrelates the time constant effect of the DC/DC converter with the performance of the algorithm. For this reason, the time scale is in samples, which can be viewed as a normalization by the update rate of the MPPT in a real application.

In these systems, perturbations come from very different natures: they can be due to measurement errors; changes in the PV I-V curve due to environmental factors (such as slow or fast varying irradiances or temperature changes); or changes in the output impedance of the DC/DC converter. This analysis was focused on the variation of the output resistance R_{out}, since it was discarded from the learning rule (assumed constant in (2)), and typically it changes over time. Yet, the controller should track the maximum power in this scenario. Consider the situation where the system has reached its optimum. If R_{out} varies, the input impedance to the PV changes, as equation (2) shows. This will in turn, change the optimum value for the system, as it will imply another voltage level. Therefore, it is desirable that the adaptive system "senses" this effect, and acts on the duty cycle in order to compensate the perturbation. An effective and easy way of assessing the tracking capability of the controller is to continuously vary the R_{out} value with a sine-wave at different frequencies and amplitudes. Therefore, R_{out} was modelled as $R_{out} = \overline{R_{out}} + \frac{r}{\overline{R_{out}}*100}\sin(\omega.n)$, where $\overline{R_{out}}$ is the DC value of the load, r is ratio of the amplitude variation with respect to $\overline{R_{out}}$ and ω is the normalized frequency.

In order to track these perturbations, the gradient magnitude over time must follow a similar shape to the variations shape, and the same holds for the frequency. Intuitively, the step-size constant adjusts how fast the controller is able to react to a perturbation, so the bigger its value is, the faster the system should be able to track these variations. Figure 6 shows the behaviour of the duty-cycle when $\overline{R_{out}} = 100\Omega$, $r = 50\%$ and $\omega = 0.01$. In the left part, ε was set to 5.10^{-5} and 10 times greater in the right part ($5 \cdot 10^{-4}$). The dashed curve in both parts represents the optimum duty cycle for the given perturbation value, while the strong curve represents the D value outputted by the controller. In the first scenario, it took approximately 2200 iterations for the controller to reach the optimum curve, as opposed to the second scenario where the speed of convergence increased significantly - since only 300 iterations were needed approximately. In the left part, although the controller is able to reach the correct amplitude according to the perturbation, the delay between the two curves is evident. The right part shows the effect of increasing the step size which leads to a significant increase in the tracking speed, where the phase angle between the controller output and the optimum is unnoticeable. However, the output noise is increased, due to the fact that the gradient estimate is noisier.

Increasing the step-size of the controller increases the stabilization speed of the system. This behaviour is shown in table IV, where the number of iterations required for the system to reach $(1-1/e)p^*$ were measured, being p^* the optimum power value. No important differences with respect to the considered frequencies were verified, hence this parameter is not present in this table. Notice that the step-sizes for both rules (being ϵ_1 and ϵ_2 the respective step-sizes for rules I and II) were set so that the time-constant is approximately the same, ensuring a proper comparison between both rules.

Table IV: Controller time constant measured for different simulated scenarios

r (%)	ε_1 ($\times 10^{-8}$)	ε_2 ($\times 10^{-5}$)	$\tau(Iterations)$
1	15	5	2178
	60	20	562
	120	50	239
	200	100	132
5	15	5	2231
	60	20	562
	120	50	238
	200	100	133
10	15	5	2365
	60	20	581
	120	50	235
	200	100	134
20	15	5	2048
	60	20	549
	120	50	233
	200	100	136
50	15	5	1427
	60	20	487
	120	50	224
	200	100	143

Table VI shows the Mean squared error (MSE) measured between the optimum duty cycle and the value actually ob-

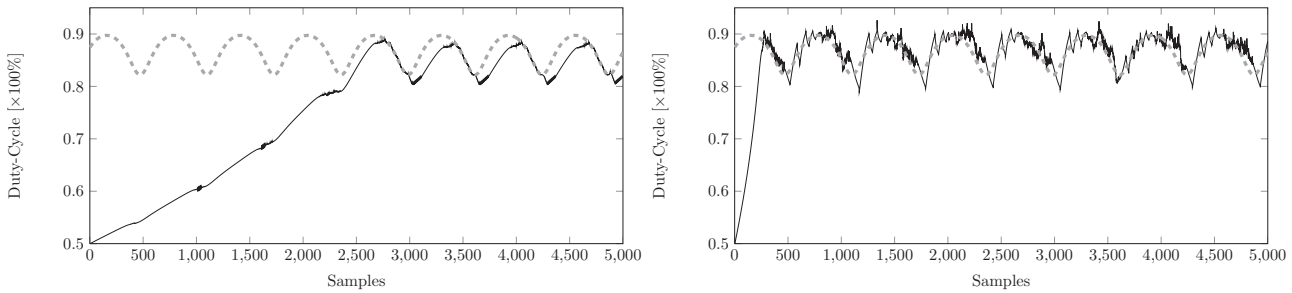

Figure 6: Duty-cycle results obtained during simulations when rule II is used. The system is being perturbed in the following way: $\overline{R_{out}} = 100\Omega$, $r = 50\%$ and $\omega = 0.01$. The left part shows the effect of choosing $\varepsilon = 5.10^{-5}$, while the right part depicts the system behaviour when $\varepsilon = 5.10^{-4}$. The gray and black curves refer respectively to the the optimum duty-cycle and the output by the MPPT converter.

tained for both rules, where the left and right tables represents respectively the results for Rules I and II . Different operating scenarios were considered, relating controller step-sizes with magnitude and frequency of the perturbation sine wave. The optimum duty cycle value was computed previously for all the perturbation scenarios. The smoothing operator used in the derivative estimate during simulations was simply the saturation operator, bounding this value within the ± 200 range. From a general point of view, the error increases as the magnitude (r) of the perturbation increases. This is due to the fact that higher amplitude variations imply greater variations in the optimum duty cycle, so the "distance" to travel is higher. Another interesting aspect to analyse is the controller behaviour with respect to the frequency. In general, for a fixed step-size value (ϵ), as the frequency is decreased (lower ω), the MSE decreases which was expected since faster variations imply higher step-sizes to ensure proper tracking. These results show that the controller tracks slow variations easily than fast variations. In order to increase the controller response, larger step sizes can be used, which would in principle improve the controller behaviour in the MSE sense. However, as observed before the introduced noise is higher, leading to an increase in the MSE value most of the times. In fact, this was expected since even without perturbations, higher step-sizes would imply higher *rattling* effects during steady-state, due to a noisier derivative estimate. This effect mimics the behaviour of conventional linear adaptive filters during adaptation [13]. Comparing the behaviour of the controller when different rules are used, one can conclude that in general the MSE in smaller when rule II is used, specially for higher rs. This shows that in addition to being smoother, Rule II handles perturbations better than Rule I. This can be explained by the fact the gradient expression is smoother.

Table V shows how the different scenarios affect the power output in terms of RMS value with respect to optimum (in percentage). Analogous observations and conclusions of those discussed for table VI can be drawn from this table. This was expected since the higher the duty cycle is from the optimum, the lower the extracted power is, and vice-versa. This table intents to show a more practical interpretation of the MSE values shown in table VI.

Table V: RULE II: RMS values with respect to the optimum power output in different simulated scenarios

r (%)	ε ($\times 10^{-5}$)	ω = 0.1	0.01	0.001	0.0001
1	5	99.8837	88.7901	99.4687	99.9941
	20	99.4591	95.4820	99.5746	99.9839
	50	99.2754	97.4146	99.5174	99.9872
	100	98.7672	97.2070	99.5760	99.9728
5	5	99.3668	88.7901	99.4687	99.9941
	20	98.4859	95.4820	99.5746	99.9839
	50	97.9618	97.4146	99.5174	99.9872
	100	97.6271	97.2070	99.5760	99.9728
10	5	98.5688	88.7901	99.4687	99.9941
	20	97.6070	95.4820	99.5746	99.9839
	50	96.6438	97.4146	99.5174	99.9872
	100	96.5136	97.2070	99.5760	99.9728
20	5	96.1383	88.7901	99.4687	99.9941
	20	95.6012	95.4820	99.5746	99.9839
	50	95.0025	97.4146	99.5174	99.9872
	100	94.1481	97.2070	99.5760	99.9728
50	5	88.6063	88.7901	99.4687	99.9941
	20	85.9593	95.4820	99.5746	99.9839
	50	32.2997	97.4146	99.5174	99.9872
	100	87.9965	97.2070	99.5760	99.9728

IV. Conclusions

A method to perform MPPT for PV panels is proposed with single variable measurement, by imposing the duty-cycle value directly in the DC/DC converter. Its derivation is done for the input voltage case but analogous results are obtained if the input current is measured. A full theoretical derivation is presented, as well as a proof of global stability around the optimum operating point for the considered cost function. The DC/DC efficiency effects were also discussed. The obtained learning rule shows very simple computational complexity as well as good speed of adaptation and converges very close to the true optimum. Simulations were carried out showing that it is robust to variations on the load impedance.

Acknowledgements

This work is supported by the ERDF through the Programme COMPETE and by the Portuguese Government through FCT - Foundation for Science and Technology, project ref. CMU-PT/SIA/0005/2009.

Table VI: MSE values with respect to the optimum duty cycle in different simulated scenarios for both rules.

r (%)	ε ($\times 10^{-8}$)	ω = 0.1	0.01	0.001	0.0001
1	15	6,15E-05	8,83E-06	1,12E-06	8,46E-07
	60	5,25E-05	1,11E-05	7,43E-06	1,19E-05
	120	9,42E-05	5,35E-05	3,32E-05	3,99E-05
	200	3,34E-04	9,97E-05	3,37E-05	8,32E-06
5	15	3,08E-04	3,30E-05	5,58E-06	6,30E-06
	60	2,15E-04	2,22E-05	1,40E-05	2,57E-05
	120	2,59E-04	1,12E-04	6,11E-05	1,33E-04
	200	5,73E-04	2,24E-04	6,97E-05	6,13E-05
10	15	5,06E-04	6,16E-05	1,49E-05	2,03E-05
	60	3,91E-04	4,66E-05	2,45E-05	4,98E-05
	120	3,82E-04	1,69E-04	1,05E-04	1,87E-04
	200	5,93E-04	2,19E-04	8,26E-05	7,32E-05
20	15	9,10E-04	1,54E-04	4,22E-05	6,03E-05
	60	6,01E-04	1,12E-04	5,39E-05	1,14E-04
	120	5,71E-03	1,90E-04	1,26E-04	1,65E-04
	200	6,07E-04	3,00E-04	1,37E-04	1,07E-04
50	15	2,28E-03	7,59E-04	1,97E-04	1,92E-04
	60	5,67E-03	6,43E-04	1,58E-04	2,72E-04
	120	1,70E-03	2,89E-04	1,44E-04	2,18E-04
	200	7,50E-03	5,18E-04	4,13E-04	8,08E-04

(a) Rule 1

r (%)	ε ($\times 10^{-5}$)	ω = 0.1	0.01	0.001	0.0001
1	5	1,15E-05	9,66E-06	2,67E-06	6,08E-07
	20	4,09E-05	1,27E-05	2,91E-06	8,59E-07
	50	6,18E-05	1,47E-05	4,14E-06	1,16E-06
	100	9,05E-05	2,28E-05	7,99E-06	3,57E-06
5	5	4,43E-05	4,12E-05	7,45E-06	1,58E-06
	20	1,06E-04	3,89E-05	8,23E-06	2,04E-06
	50	1,79E-04	4,15E-05	1,06E-05	3,78E-06
	100	2,35E-04	5,58E-05	1,66E-05	6,26E-06
10	5	1,09E-04	8,73E-05	1,61E-05	2,91E-06
	20	1,82E-04	6,71E-05	1,24E-05	3,31E-06
	50	2,95E-04	6,56E-05	1,63E-05	4,92E-06
	100	3,84E-04	9,01E-05	2,43E-05	7,68E-06
20	5	3,32E-04	2,89E-04	1,73E-05	4,65E-06
	20	3,70E-04	1,23E-04	2,14E-05	4,80E-06
	50	4,83E-04	1,08E-04	2,49E-05	7,70E-06
	100	5,90E-04	1,31E-04	3,78E-05	1,06E-05
50	5	1,31E-03	1,33E-03	6,26E-05	7,52E-07
	20	1,72E-03	5,45E-04	5,94E-05	1,67E-06
	50	4,73E-03	3,04E-04	4,73E-05	1,92E-06
	100	1,74E-03	3,16E-04	6,68E-05	3,15E-06

(b) Rule 2

Table VII: RMS values with respect to the optimum power output in different simulated scenarios for both rules.

r (%)	ε ($\times 10^{-8}$)	ω = 0.1	0.01	0.001	0.0001
1	15	99,17146	99,87876	99,98853	99,9886
	60	99,31641	99,85188	99,88624	99,83776
	120	98,74026	99,2699	99,51025	99,18108
	200	96,9683	98,94164	99,6107	99,91634
5	15	95,72015	99,61107	99,93575	99,88937
	60	97,0244	99,69469	99,78967	99,60048
	120	96,57991	98,51121	99,12256	98,35294
	200	94,12113	97,75713	99,3459	99,19101
10	15	93,07576	99,16796	99,81302	99,61751
	60	94,50079	99,34032	99,62675	99,13787
	120	94,93197	97,69514	98,80876	97,34066
	200	93,75753	97,7531	98,9689	98,78513
20	15	88,14057	97,9627	99,41223	98,75847
	60	92,17633	98,35925	99,1422	97,74812
	120	31,09372	97,38775	98,32442	97,94861
	200	93,27015	96,70684	98,49976	98,34358
50	15	80,33152	91,9081	97,49027	95,13922
	60	32,29971	93,48075	97,30573	94,41066
	120	85,55564	96,23209	97,60749	95,44052
	200	32,29971	93,47364	93,98928	81,31823

(a) Rule 1

r (%)	ε ($\times 10^{-5}$)	ω = 0.1	0.01	0.001	0.0001
1	5	99.8837	88.7901	99.4687	99.9941
	20	99.4591	95.4820	99.5746	99.9839
	50	99.2754	97.4146	99.5174	99.9872
	100	98.7672	97.2070	99.5760	99.9728
5	5	99.3668	88.7901	99.4687	99.9941
	20	98.4859	95.4820	99.5746	99.9839
	50	97.9618	97.4146	99.5174	99.9872
	100	97.6271	97.2070	99.5760	99.9728
10	5	98.5688	88.7901	99.4687	99.9941
	20	97.6070	95.4820	99.5746	99.9839
	50	96.6438	97.4146	99.5174	99.9872
	100	96.5136	97.2070	99.5760	99.9728
20	5	96.1383	88.7901	99.4687	99.9941
	20	95.6012	95.4820	99.5746	99.9839
	50	95.0025	97.4146	99.5174	99.9872
	100	94.1481	97.2070	99.5760	99.9728
50	5	88.6063	88.7901	99.4687	99.9941
	20	85.9593	95.4820	99.5746	99.9839
	50	32.2997	97.4146	99.5174	99.9872
	100	87.9965	97.2070	99.5760	99.9728

(b) Rule 2

REFERENCES

[1] C. Sullivan and M. Powers, "A high-efficiency maximum power point tracker for photovoltaic arrays in a solar-powered race vehicle," in *Power Electronics Specialists Conference, 1993. PESC '93 Record., 24th Annual IEEE*, pp. 574 –580, jun 1993.

[2] A. F. Boehringer, "Self-adapting dc converter for solar spacecraft power supply selbstanpassender gleichstromwandler fr die energieversorgung eines sonnensatelliten," *Aerospace and Electronic Systems, IEEE Transactions on*, vol. AES-4, pp. 102 –111, jan. 1968.

[3] J. J. Schoeman and J. D. van Wyk, "A simplified maximal power controller for terrestrial photovoltaic panel arrays," in *PESC '82; 13th Annual Power Electronics Specialists Conference*, pp. 361–367, 1982.

[4] G.-J. Yu, M. woong Jung, J. Song, I.-S. Cha, and I.-H. Hwang, "Maximum power point tracking with temperature compensation of photovoltaic for air conditioning system with fuzzy controller," in *Photovoltaic Specialists Conference, 1996., Conference Record of the Twenty Fifth IEEE*, pp. 1429 –1432, may 1996.

[5] R. Ramaprabha, B. Mathur, and M. Sharanya, "Solar array modeling and simulation of mppt using neural network," in *Control, Automation, Communication and Energy Conservation, 2009. INCACEC 2009. 2009 International Conference on*, pp. 1 –5, june 2009.

[6] T. Kitano, M. Matsui, and D. hong Xu, "Power sensor-less mppt control scheme utilizing power balance at dc link-system design to ensure stability and response," in *Industrial Electronics Society, 2001. IECON '01. The 27th Annual Conference of the IEEE*, vol. 2, pp. 1309 –1314 vol.2, 2001.

[7] F. Huang, G. Zhimin, T. Forughian, and D. Tien, "A new microcontroller based solar energy conversion modular unit," in *Power Conversion Conference - Nagaoka 1997., Proceedings of the*, vol. 2, pp. 697 –700 vol.2, aug 1997.

[8] T. Esram, J. Kimball, P. Krein, P. Chapman, and P. Midya, "Dynamic maximum power point tracking of photovoltaic arrays using ripple correlation control," *Power Electronics, IEEE Transactions on*, vol. 21, pp. 1282 –1291, sept. 2006.

[9] A. Ali, M. Saied, M. Mostafa, and T. Abdel-Moneim, "A survey of maximum ppt techniques of pv systems," in *Energytech, 2012 IEEE*, pp. 1 –17, may 2012.

[10] A. Driesse, S. Harrison, and P. Jain, "Evaluating the effectiveness of maximum power point tracking methods in photovoltaic power systems using array performance models," in *Power Electronics Specialists Conference, 2007. PESC 2007. IEEE*, pp. 145 –151, june 2007.

[11] J. C. Principe, N. R. Euliano, and W. C. Lefebvre, *Neural and adaptive systems: fundamentals through simulations*. Wiley New York, 2000.

[12] G. Kostakis, S. Manias, and N. Margaris, "A generalized method for calculating the rms values of switching power converters," *Power Electronics, IEEE Transactions on*, vol. 15, pp. 616 –625, jul 2000.

[13] J. C. Príncipe, N. Euliano, and W. Lefebvre, *Neural and adaptive systems: fundamentals through simulations*. Wiley, 2000.